AIAA 81-0521R

Attenuation of Propeller-Related Vibration and Noise

J.F. Johnston* and R.E. Donham†
Lockheed-California Company, Burbank, California

The potential sources and paths by which the propeller produces structural responses resulting in vibration and noise in the cabin of a transport aircraft are discussed. New low-cost, convenient experimental and analytical techniques are described for evaluating the excitations—propeller airborne pressures on the fuselage shells, slip-stream-induced forces on the wing and tail, and oscillatory forces on the propeller. The techniques described make use of ground-determined structural signatures to relate forces with vibrations or noise, and of propeller signatures from flight tests which define the vibroacoustic contributions of individual propellers. Knowing these, the propeller-produced excitation forces can be deduced by the relations shown; design approaches to control the fatigue and vibroacoustic environment can then be enunciated logically.

Introduction

THE airlines of the world are currently facing an ever-increasing amount of pressure due to the high cost of fuel. This pressure has already forced the older, less efficient jet transports into retirement. The newer turbofan transports are still not efficient enough to remove the profit squeeze due to fuel costs. Newer, high-pressure-ratio core engines will further reduce turbofan fuel consumption (Fig. 1). The same core engine technology applied to an advanced turbopropeller system, however, will further reduce that low fuel consumption by 15% while maintaining cruise speeds in the Mach 0.7-0.8 range. This fuel efficiency puts the advanced turboprop aircraft into the front rank for consideration as next-generation commercial and military transports.

The technical problems in developing and using the advanced turboprop propulsion system are addressed in a NASA Aircraft Energy Efficiency (ACEE) program. Its progress is described in Ref. 1. A significant part of that program is to make the internal vibration and noise environments competitive with those of turbofan aircraft.

Vibration and noise are closely related, inasmuch as vibrations of the fuselage shell and floor produce the noise heard in the cabin. The tentatively established noise control goal listed below has been found to set the vibration control goal as well, as plotted in Fig. 2. The noise control goals are to keep the noise within 93 dB OASPL (overall sound pressure level); 80 dB(A) (A-weighted noise level); 65 dB SIL (speech interference level).

The A-weighting is intended to reflect human ear sensitivity. It downgrades the low frequencies (below 1000 Hz), and gives greater weighting to the 1-, 2-, and 4-kHz ranges, in summing the A-weighted energies in all octave bands. The SIL is simply the average of the dB readings of the 1-, 2-, and 4-kHz octave bands.

From the above, the corresponding vibration control goals are set at those levels which can produce a noise level no higher than 90 dB in any one octave band; 75 dB(A) in any one octave band; 65 dB SIL in any one octave band.

From Fig. 2, the 90-dB/octave portion limits allowable vibrations below about 135 Hz, the A-weighted portion limits from there to just below 1 kHz, and the SIL limits vibrations at and above 1 kHz. These limits are associated with vibration levels that lie between perceptible and unpleasant in the rankings of Goldman.[2] They can be considered competitive with current turbofans (shaded area), but must be lower by a factor of about 8; (i.e., down 18 dB) from the limits found in current turboprops.

This large reduction, against the background of a more hostile environment in terms of propeller torque and advancing tip Mach number, indicates that every source and every path by which vibration and noise enter the cabin must be considered.

Until recently, we have dealt with the most obvious source, the oscillatory pressures on the fuselage shell, airborne from the adjacent propeller. Recent work in this area, centered around the Hamilton Standard Prop-Fan, is reported in Refs. 3-7. Recent analysis of flight test data, as in Ref. 8, has indicated, however, that part of the noise and much of the vibration is due to propeller slip-stream excitations of the wing and tail, structure-borne into the cabin floor and shell.

It is toward the understanding and evaluation of all these excitations and their structural and vibroacoustic effects that this paper is addressed. New experimental and analytical techniques are described for evaluating the propeller input forces on the fuselage shell, the slip-stream-induced forces and moments on the wing and tail, and the contributions of each, separately, to the structural responses, including the noise and vibration in the cabin. With the excitation forces and responses evaluated in magnitude and phase, design approaches to controlling structural fatigue and the vibroacoustic environment can be enunciated logically.

Discussion

Input Source/Path Matrix

The sources and paths that need to be considered in determining the vibroacoustic environment are listed in Table 1.

Airborne

Most of the work has been concentrated on the first listed source, the airborne pressures from the propeller acting on the fuselage shell. Recent excellent work has been done in source prediction, as represented by Refs. 9-11. Source analysis/test correlations,[7,12] show encouraging results. Predictive and test work is needed on the effects of nonuniform inflow on near field and far field noise, however.

Large-scale capabilities in structural finite-element and acoustic modes analysis, as represented by Refs. 13 and 14, are well suited to use the source predictions. When these capabilities are extended and combined, structural and

Presented as Paper 81-0521 at the AIAA/ASME/ASCE/AHS 22nd Structures, Structural Dynamics and Materials Conference, Atlanta, Ga., April 6-8, 1981; submitted April 8, 1981; revision received Jan. 4, 1982.

*Senior Research and Development Engineer, retired.
†Group Engineer, Dynamics and Vibration. Member AIAA.

Table 1 Propeller-induced vibration and noise

Source	Path	Remarks	Source analysis: Prediction	Source analysis: Correlation with test	Path analysis: Prediction	Path analysis: Correlation with test	Status
Airborne pressures on shell	Through shell and trim	Primary noise source, high harmonic content, shell vibration affects comfort, fatigue, equipment	Succi/Farassat, Hanson, Runyan (axial flow only; needs extension to nonuniform inflows)[b]	Excellent to good[a,b]	Finite element[b] Generalized shell structure	Good[b] Good to poor	Good, relatively new Fair
Slip-stream over wing	Through wing to shell and floor	Primary vibration source, probable important noise source, lower harmonics	No published papers[a]	Need test data[a]	Finite element required[b]	None[b]	Needs work—test and prediction
Slip-stream over tail	Through tail to shell and floor	Fatigue failures obstacles 7-9-dB noise reduction when tail out of slip-stream (general aviation aircraft)	No published papers[a]	Need test data[a]	Finite element required[b]	None[b]	Needs work—test and prediction
Forces on propeller	Through hub, nacelle, and wing to shell and floor	Can be significant; aeroelasticity may amplify	No published papers[a]	Need test data[a]	Finite element required[b]	None[b]	Needs evaluation
Multiple-propeller effects	All the above	Relative prop phase important, up to 8:1 variation in total acoustic energy	Vector sum of above; requires phase predictions	Prop and tap signatures[a]	Vector sum of above; requires phase predictions[b]	Good using prop signature techinque[a]	Good—handle with prop signature technique

[a] Addressed herein. [b] Work needed.

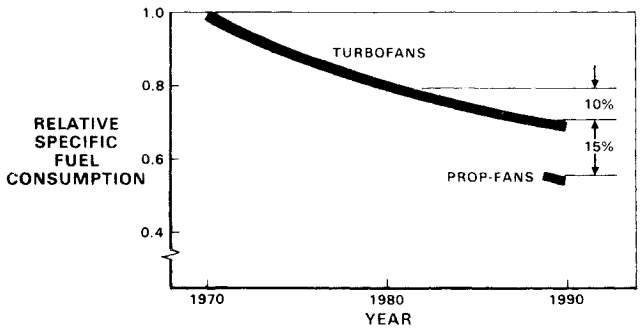

Fig. 1 Expected turboprop (prop-fan) and turbofan fuel efficiencies Mach 0.8 at 35,000 ft.

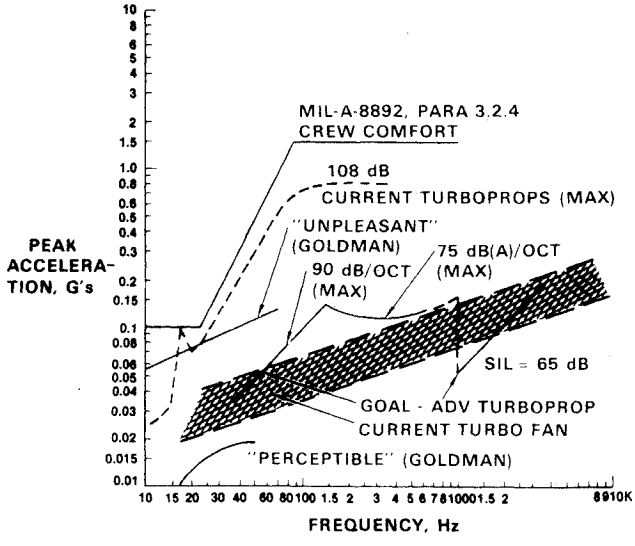

Fig. 2 Vibration levels.

acoustic response prediction for airborne propeller excitations will be in excellent shape for design use.

The other sources and paths are little known, in spite of scattered indications that they may be quite significant.

Wing in Slip-stream

Physical reasoning (and occurrence of wing leading-edge cracks behind the propeller) indicates that the oscillatory slip-stream forces on the wing can be quite large. The air swirl behind the propeller contains all of the propeller torque, in packets of swirl behind each blade. The wing, in straightening out virtually all the vertical component of the swirl velocity, reabsorbs almost half the propeller torque. The NASA advanced turboprop activity[1] is sponsoring testing for the effects of the swirl on the optimization of the integrated prop-nacelle and wing. An order-of-magnitude estimate of the ratio of oscillatory torque to mean torque absorbed by the wing, obtained by simple lifting line analysis of the propeller wake, is shown in Fig. 3. This was done for unswept blades, like those for the P-3 (four blades) or the eight-bladed SR-2 Prop-Fan, Fig. 4 (see Ref. 1). The oscillatory inputs decrease from a relatively sharp impulsive-type input shown in Fig. 3 for a two-blade propeller to smaller values as the number of blades increases. For a prop-fan with ten straight blades the oscillatory component would be about 10% of the torque absorbed by the wing, or about 5% of the mean propeller torque. This ±5% oscillatory component would still be very significant—about ±1600 ft-lb at about 200 Hz behind each

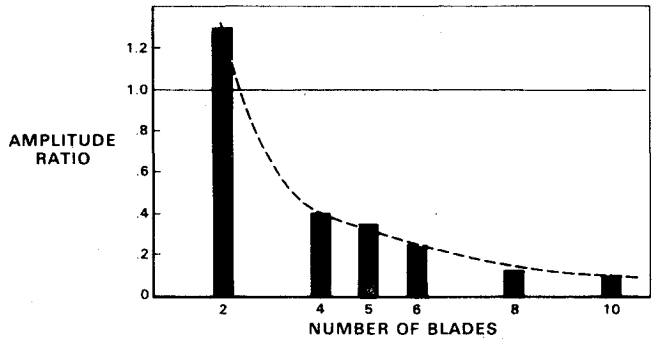

Fig. 3 Estimated ratio of oscillatory torque to mean torque absorbed by wing.

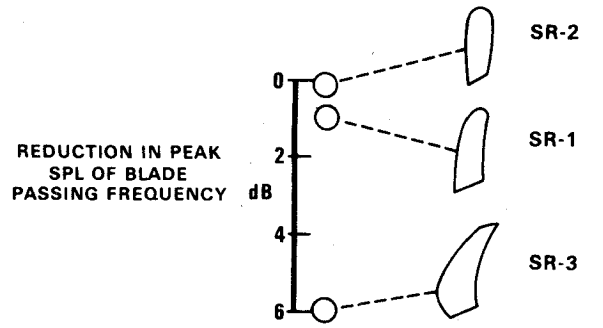

Fig. 4 Noise comparison of three propeller models; Lewis 8×6 Wind Tunnel, Mach 0.8 design conditions.

propeller of a twin-engine, 120,000-lb gross weight transport cruising near Mach 0.8 at 30,000 ft. Such inputs can be important to structural fatigue considerations for the wing and empennage. Significant aerodynamic amplification and fatigue damage can result if hinged surfaces such as ailerons, elevators, and tabs are in the slip-stream. Unless the inputs could be very effectively balanced/cancelled by synchrophasing, they would be expected to produce significant vibration and noise in the cabin.

Fortunately the prop-fan to be used will be more like the SR-3 with swept blades (Fig. 4), in which the effect of sweep will be to smooth out the swirl over the wing. Even with blade sweep, however, the slip-stream excitation of the wing is expected to remain an important factor.

Tail in Slip-stream

Tail excitation by the slip-stream is also important. In general-aviation aircraft, cases have been reported where changing from a conventional tail to a T-tail configuration, thus moving the horizontal tail out of the slip-stream, resulted in reducing cabin noise by 7-9 dB. Fatigue cracking of stabilizer primary structure, leading edges, elevator and tab actuator support structure and fittings has been reported; some of these led to fatal accidents. Note that these severe excitations occurred after the wing had removed about half the oscillatory swirl. In a larger aircraft, the P-3C, tap tests on the stabilizer root resulted in surprisingly large noise transfer into the forward cabin, again showing the potential importance of slip-stream over the tail. The effects of slip-stream excitation may well lead to choice of a T-tail configuration for propeller-powered transports.

Prop Forces

The fourth item in the source/path matrix, oscillatory forces on the propeller itself, is difficult to estimate. Nonuniform inflow due to angle of attack will produce significant once-per-revolution (1*P*) loads on the blade, and curved flow will cause 2*P* blade loads. While these modify the airborne pressures on the shell, the 1*P* loads are not transmitted as oscillations into the mounts if the prop has more than two blades, and the 2*P* loads are not transmitted as oscillations if the prop has more than three blades. A four-blade prop will transmit 4*P* oscillations from 3*P*, 4*P*, and 5*P* blade loads, and a ten-blade prop will transmit 10*P* oscillations from 9*P*, 10*P*, and 11*P* blade loads. The higher-frequency blade load content exists for nonlinearities producing impulsive-type inputs, such as blade passage through locally nonuniform airflow or discontinuous occurrences like blade stall or shock-induced separation in part of the blade load cycle.

The effect of fuselage cross flow on the P-3 at 2-deg angle of attack, representing a locally nonuniform airflow over the inboard prop as the blade passes nearest the fuselage, has been estimated. The disturbance produces 4*P* hub vertical and thrust forces estimated at ±15-25 lb at cruise, and 4*P* yawing moments of order ±75-125 ft lb. The level of vertical force is not considered important, but the effects of the yawing moment and thrust variations have not been evaluated.

For a ten-blade prop-fan, the same inflow nonuniformity due to fuselage cross flow (no increase in clearance) would produce about ±1.5 lb of 10*P* thrust or vertical force variation, or about ±10 ft-lb of 10*P* yawing moments from a rigid propeller. These are probably negligible, but here dynamic-aeroelastic blade responses could be large enough to make the propeller forces important.

Multiple Props

The source/path matrix of Table 1 is completed by noting multiple propeller effects. These may be additive or subtractive, depending on the relative phases of the propellers. Multiple propeller effects are noted here to point up the importance of phase in both predictions and tests. This importance is underscored in Ref. 8 by noting that no future vibroacoustic tests should ever be made in a propeller-powered airplane without recording and accounting for the propeller phase angles.

In summary, Table 1 makes the following points:

1) Of the four vibroacoustic source/path systems listed, the first, oscillatory pressures on the fuselage shell, is important and is well understood, but source prediction methods require extension to the effects of nonuniform inflow.

2) Test/analysis correlations are expected to improve when the above source predictions are combined with large-scale, finite-element structural and internal acoustic mode descriptions.

3) Oscillatory slip-stream excitations of the wing and tail are important, are not well understood, and require theoretical prediction work, test work, and test/analysis correlation. Finite-element structural techniques are useful here as well.

4) Oscillatory excitations of the propeller are probably less important as inputs to the wing and shell, but are not well enough understood. Test work is in order here, preferably on full-scale articles where the blade dynamic-aeroelastic responses can be represented.

5) Multiple-propeller effects are very important. Recently developed propeller signature techniques based on test data have proved valuable here, and promise to be one of the tools by which the other source/paths can be evaluated.

Propeller signatures are discussed in the following section.

Propeller Signatures

Each propeller in a multipropeller aircraft contributes differently to the noise and vibration in the aircraft. The individual propeller contribution at any location is called its signature at that location. It consists of complex waves having components at frequencies equal to the blade passage frequency, *NP* (*N* is the number of blades, *P* stands for per

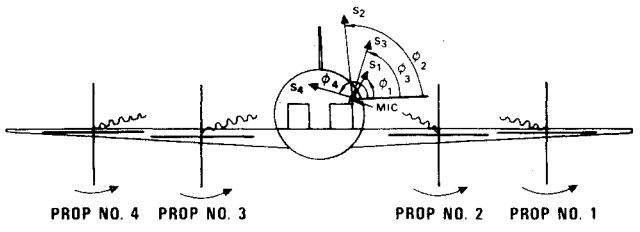

Fig. 5 Propeller signatures.

revolution), and integer multiples of the blade passage frequency, *kNP*, where *k* is an integer. In this discussion the magnitude and phase of a given frequency component of the contribution will be called its signature at that frequency. This signature can be determined from test data.

Figure 5 is an illustration of signature vectors for noise at a specific location in a four-engine airplane. The sound pressure vectors S_1, S_2, S_3, and S_4 arrive from similarly numbered propellers. The length of each vector represents the pressure amplitude at that location due to that propeller. The phase $\phi 1$, $\phi 2$, etc., is the fraction of the wavelength by which the vector leads the propeller "pip" which marks the propeller passing the reference position. Inasmuch as the *kNP* wave pattern repeats itself *kN* times per revolution, the vector rotates *kN* deg for every degree of propeller rotation (Fig. 6). For a four-bladed propeller the 4*P* vector rotates 4 deg per degree of propeller rotation, the 8*P* vector rotates 8 deg per 1 deg, etc. In Figs. 5 and 6 the propeller reference position is blades-level. The actual position may be arbitrary, as long as it is the same for all propellers.

The signatures or influence vectors add as shown in Fig. 6, which represents the 4*P* components. For propeller phase angles on the left, the vectors nearly close, giving a low net pressure amplitude of 0.024 psf, or 96 dB. A 20-deg retardation of the No. 2 propeller (an 80-deg retardation of its signature vector) and a 15-deg advance of the No. 3 propeller (60-deg advance of its vector) as shown on the right, result in a much larger net vector, 0.15 psf, 111 dB. It is apparent from this example that the effect of the relative propeller phasing is important and can be calculated easily when the signatures are known.

To determine the signatures from test data, it is, in theory, necessary only to measure the sound pressure (or vibration) vector at four different known combinations of propeller phases to find the signatures. In practice the accuracy is improved by using more data points in a least-squares determination, which is included in the computer code LOCKPHASE, a FORTRAN program developed for signature analysis.

The basic equation assumes local linearity, i.e., that the contribution of each propeller is vectorially additive in arriving at the net noise or vibration at a given position. In complex notation, and using the No. 1 propeller as the reference for phase, the 4*P* noise (as an example) is divided into "real" (cosine) and "imaginary" (sine) components.

$$A_R = A_m \cos\phi_m = S_1 \cos(\phi_1) = S_2 \cos(\phi_2 + 4\psi_2) + S_3 \cos(\phi_3 + 4\psi_3) + S_4 \cos(\phi_4 + 4\psi_4)$$

$$A_I = A_m \sin\phi_m = S_1 \sin(\phi_1) + S_2 \sin(\phi_2 + 4\psi_2) + S_3 \sin(\phi_3 + 4\psi_3) + S_4 \sin(\phi_4 + 4\psi_4)$$

See Figs. 5 and 6 for definition of terms. The A_m, ϕ_m, and ψ_2, ψ_3, ψ_4 are measured test data; the signatures S_n, ϕ_n are to be determined. The 4ψ terms are replaced by 8ψ or 12ψ when dealing with the 8*P* or 12*P* signatures, respectively.

Expansion of the trigonometric terms allows separation of variables into separate matrices for the sound pressures (or vibrations), $[A]$, the sines and cosines of ψ, $[\psi]$, and the signatures, $[S]$. In matrix notation, the equations become

$$[A] = [\psi]\,[S]$$

The least-squares form for use with more than the minimum data sets is obtained by premultiplying both sides by $[\psi]^T$, the transpose of the (nonsquare) ψ matrix. Solution for the signatures then follows by premultiplying both sides by $[[\psi]^T[\psi]]^{-1}$, the inverse of the resulting square matrix of ψ. This gives

$$[S] = [[\psi]^T[\psi]]^{-1}[\psi]^T[A]$$

Details are contained in Ref. 8.

Test Signatures

As reported in Ref. 8, the signatures measured on a Navy/Lockheed P-3C four-propeller patrol aircraft were validated by using them to predict the noise levels at 12 test locations for later test runs at the same altitude and speed. Examples are shown in Figs. 7 and 8 for two microphones in the cabin just forward of the plane of rotation. As may be seen, the test/prediction agreements are excellent for all three runs, even Run G, taken about three weeks later, in which the outboard engines were feathered. The prediction was made by zeroing the signatures for the two outboard engines, No. 1 and No. 4.

The calculated strong effects of synchrophasing are shown (also from Ref. 8) in Fig. 9 for the noise and in Fig. 10 for the

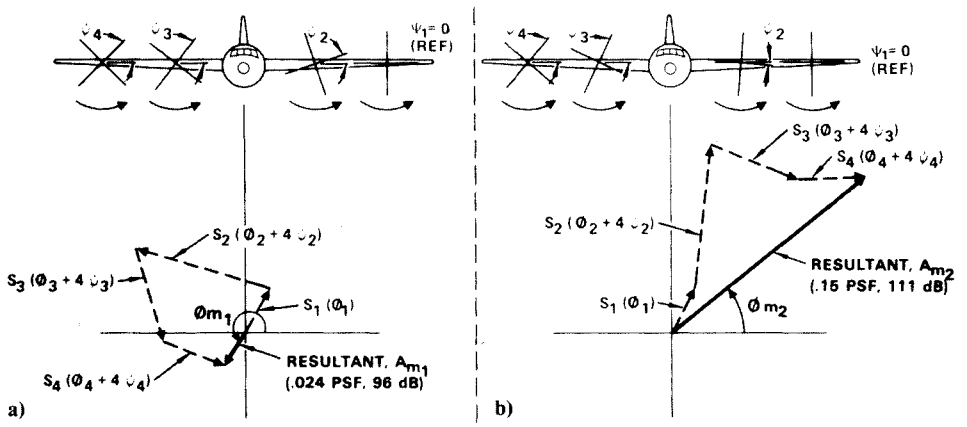

Fig. 6 Addition of signatures 4*P* components. a) Test sample No. 1. b) Test sample No. 2.

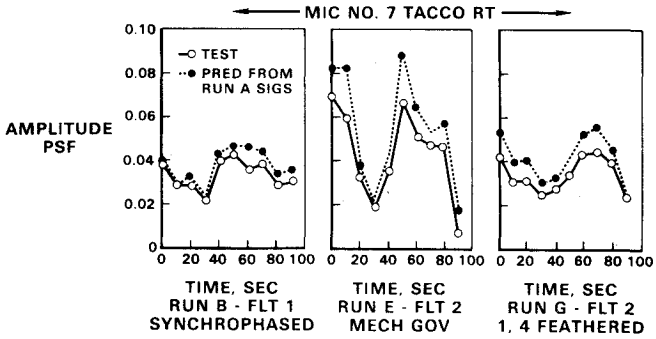

Fig. 7 $4P$ noise prediction, MIC 7.

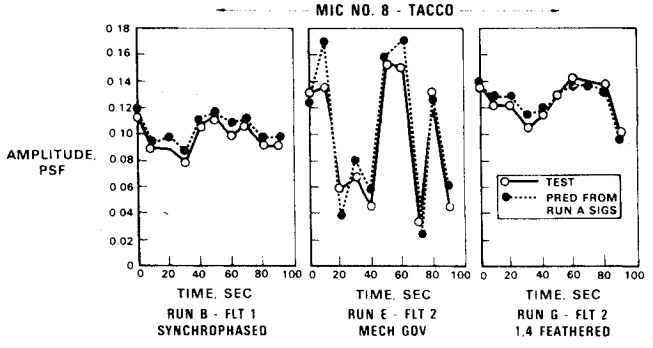

Fig. 8 $4P$ noise prediction, MIC 8.

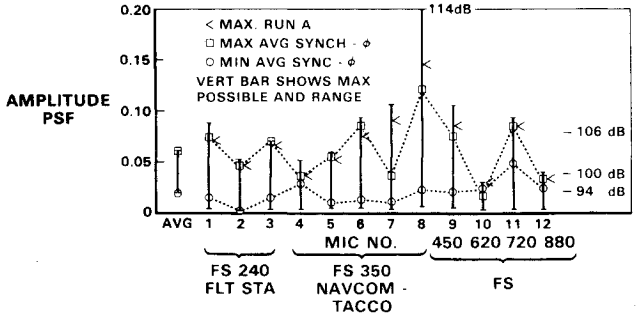

Fig. 9 Synchrophase effect on 68-Hz noise.

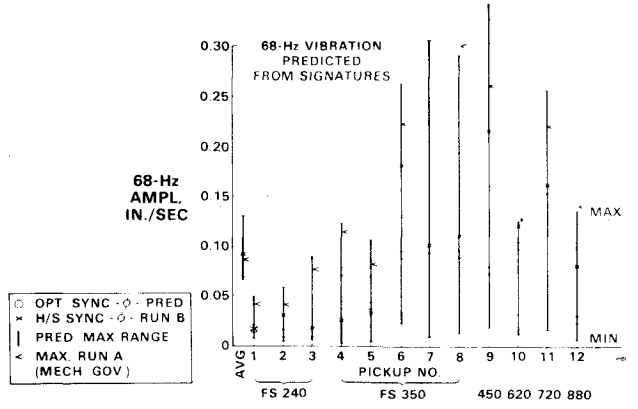

Fig. 10 Synchrophase effect on 68-Hz vibrations.

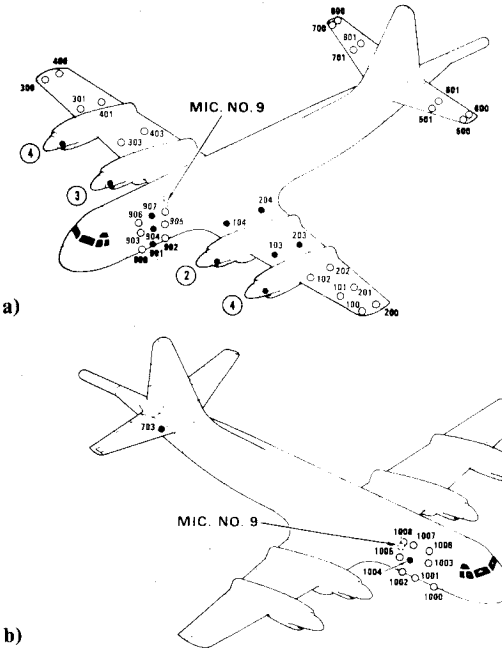

Fig. 11 P-3C tap test input points; a) left side; b) right side.

vibrations at 12 locations. The synchrophase sets that produced the lowest and highest average predicted sound pressures also produced the lowest and highest predicted average vibration levels—a not unexpected occurrence. It is important to note that synchrophase produced an overall reduction of noise and vibration, not just a redistribution.

Additional conclusions on propeller signatures from Ref. 8 follow.

1) Outboard propellers are significant contributors to the noise and vibration in the fuselage (pointing up the probable importance of the wing-borne excitations).

2) Smaller synchrophase errors (than the observed ±5-deg phase oscillations) are desirable to achieve optimum noise/vibration conditions; the eight- and ten-blade prop-fans will require still more accuracy.

3) Much of the wide variability of noise measurements for a given multipropeller airplane can be attributed to differences in phase angles: no future propeller-powered airplane vibroacoustic tests should ever be made without accurately measuring and accounting for the relative propeller phase angles.

Although the use of propeller signatures has an immediate payoff in its ability to predict optimum phase angles for minimum overall or weighted sound and vibration levels, its most promising use is as a tool for separating and evaluating the vibroacoustic source and path systems discussed in Table 1. In this respect they are used in conjunction with structural signatures, as described in the following section.

Structural Signatures

"Structural signature" is a convenient name to describe the frequency response of motion, vibration, or noise at one point in a structure to a unit force applied at the same or another point in the structure; it is a transfer function characteristic of the structure between those points. In this discussion the interest centers on the use of ground-determined structural signatures to deduce forces applied in flight by the propellers. If the vibration/noise pattern due to the propeller is known from flight test, and if the forces required to produce that vibration/noise pattern are known from ground structural signature tests, then the excitation forces due to the propeller are determinable.

A number of test techniques are available to determine structural signatures, as discussed, for example, in Ref. 15. The oldest, and considered most accurate, is steady-state excitation at a sufficient number of discrete frequencies and excitation points. This technique is so laborious that it is

seldom used. Swept-sine techniques were introduced. The advent of the modern computer and the Fast Fourier Transform (FFT) made other forms of excitation practical. Pure random, periodic random, and pseudorandom excitations and "chirps" (logarithmically swept sines of short duration) still required electromechanical or hydraulic shakers. The slow sinusoidal excitations had the advantage that they could inject relatively large amounts of energy into the structure, giving high signal-to-noise ratios; by changing amplitudes or by preloading, they could also investigate structural nonlinearities. However, the number of points to be excited (in determining excitation forces due to propellers) is necessarily large. This fact makes the use of shakers impractical from a number of considerations; difficulty of setup, time span, cost, length of aircraft tie-up, and unwillingness of engine and propeller manufacturers to warrant their product after exposure to continuous sinusoidal excitation.

Transient tests using impacts as the means of excitation are a practical alternate to the use of shakers for reasonably linear structures. This is a very fast method, in which a hand-held mallet with a load cell in the head is used to impact the structure. The input force signal is a short-duration impulse having a relatively broad frequency spectrum, depending on the material of the head—usually hard rubber or plastic. Reference 16 treats impulse techniques extensively.

From Refs. 15 and 16, it is concluded that reasonably accurate transfer functions are obtained from transient tests if

1) the results of a number of taps are added linearly until the coherence of the sum is very near 1.0 over the frequency range of interest; this provides a high signal-to-noise ratio (random noise tends to cancel out over a number of taps); high coherence also proves linearity;

2) any taps showing "overload" in either the force or response are not included in the above summation; Ref. 15 indicates large errors at resonant peaks if "clipping" occurs, although the reference shows that the accuracy away from resonance is good unless "modal analysis"‡ techniques are used.

Modern portable analysis machines such as the HP 5420A Digital Signal Analyzer perform the linear summation of accepted taps and can show coherence vs frequency after each acceptance. Tap results are not accepted by a good experimenter if an overload is indicated or if the force time history is poor or shows double impacts. Tap results are added until the coherence appears to be 1.0 over the desired frequency ranges.

Experimental Structural Signatures

An exploratory test was conducted at Lockheed in May 1980 to determine whether and under what conditions tap signatures can be used to determine vibroacoustic transfer paths, in lieu of the alternative more difficult ground vibration tests.

The airplane was a production P-3C. A single microphone was placed at midcabin just behind the prop plane. Multiple taps were performed at the 13 positions shown in Figs. 11a and 11b, using a light (½-lb) hammer. Transfer functions and coherence are shown in Fig. 12 for taps on the shell (point 901 of Fig. 11), in Fig. 13 for taps at the wing root (point 204), and in Fig. 14 for taps at stabilizer root (point 703). The coherence was good for the shell taps, but poor for the wing root and stabilizer taps, indicating need for greater input forces at the latter locations. A later repeat test with taps at the wing root using a heavier hammer (about 3 lb) showed excellent coherence (Fig. 15). The transfer function phase data are also shown in Fig. 15. The phase from 40 to 330 Hz

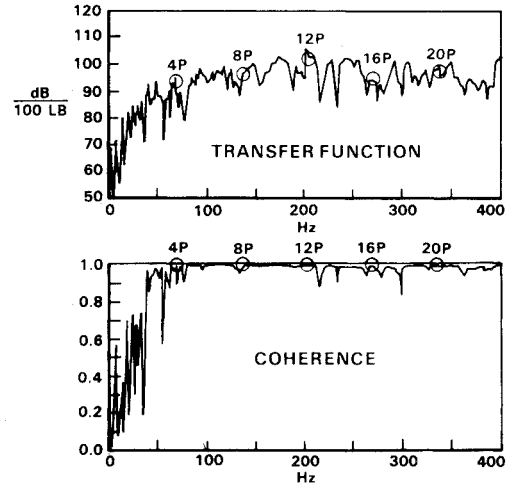

Fig. 12 MIC 9 tap signature tap at shell (point 901).

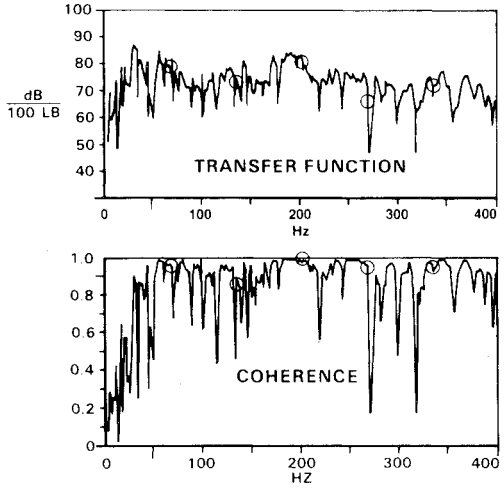

Fig. 13 MIC 9 tap signature tap at wing root (point 204).

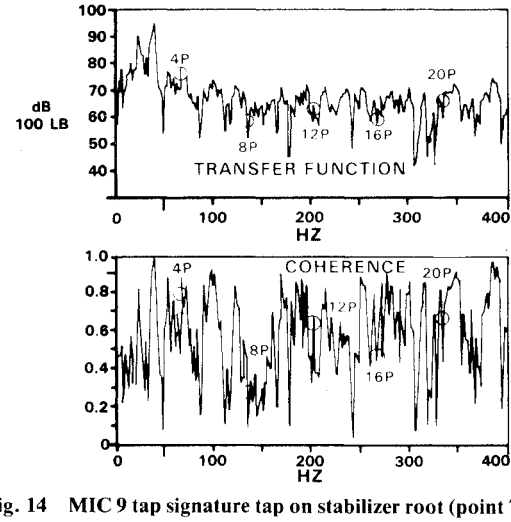

Fig. 14 MIC 9 tap signature tap on stabilizer root (point 703).

‡Given a linear system, modal analysis is a powerful tool for extending limited test data by the assumption of modal properties defined by the measured responses. It is most accurate at resonances, and is therefore useful for broadband excitations. It loses accuracy away from resonance, and is therefore questionable for the pure-tone excitations associated with propellers. The final airplane structure must of necessity be nonresonant at the important propeller frequencies. Modal analysis was not intended for the inverse problem considered here, that of determining excitation forces from measured responses.

appears well behaved, with an average rate of phase change of between 4 and 6 deg/Hz. The response of a floor-mounted vibrometer, not shown, also showed excellent coherence. Figure 15 shows raw data, inasmuch as the microphone was not calibrated. The transfer functions are not comparable between Figs. 13 and 15.

It was concluded from these simple tests that transient inputs can be used to investigate vibration and noise transfer functions and transfer paths with such apparently linear systems as the P-3 structure. The precautions taken for this test should continue to be observed, e.g., to select conditions of low ambient noise level, to make on-the-spot analyses with portable analyzer equipment to check the quality of the data, to select hammer masses appropriate to the local mass being excited, and to make multiple taps at each location to maximize the signal, rejecting taps showing overloads or poor input force time history. The primary check on the data quality is the coherence.

The remainder of the discussion will assume the use of tap-type excitations, and will call the resultant transfer functions tap signatures.

Analysis of Data

Direct Force Analysis

The direct determination of excitation forces due to propellers is illustrated in Fig. 16 as potentially applied to a P-3C. Structural signatures from vibrometers are combined with flight-determined propeller signatures to determine the force at each vibrometer location due to each propeller separately. Vibrometers placed on the fuselage shell determine the airborne forces from the propellers; vibrometers on the tail determine the slip-stream-induced excitations there; and vibrometers placed on the wing determine the oscillatory slip-stream forces on the wing. The force-response to transfer functions are determined by ground signature tests. Given the transfer functions between force and response from this ground test, the in-flight forces can be determined from the in-flight responses.

The in-flight forces, however, are generally not associated with a single propeller. It is necessary to use the propeller signature analyses,[8] to determine the separate contributions of each propeller to the response of each vibrometer. This requires that the in-flight responses be measured at about six combinations of relative propeller phase angles. The experimental and analytical treatments for propeller signatures are described in detail in Ref. 8.

In the ground test, forces are applied at positions selected to represent the propeller or slip-stream force applications, see Fig. 16. The responses are measured at the same locations. At a given frequency,

$$R_{ij}=F_j T_{ij} \tag{1}$$

where R_{ij} is the measured response at i, due to force at j (complex); F_j is the measured applied force at j, in pounds (complex); T_{ij} is the complex transfer function between R_i and F_j, in grams per pound, etc., having amplitude T_{ij} and phase ϕ_{ij}; and ϕ_{ij} is the phase angle by which response R_i leads force F_j.

The in-flight responses at a given frequency are the sum of those due to forces at the sensor (the self term) and those due to all other forces on the airplane at the same frequency,

$$R_i=\Sigma F_j T_{ij} \quad \text{including} \quad i=j \tag{2}$$

Here a decision must be made: inasmuch as there are not enough sensors to define "all other" forces on the airplane, how are we to solve for F, the desired quantity? The simplest is just to assume that the self term $F_i T_{ii}$ is large with respect to

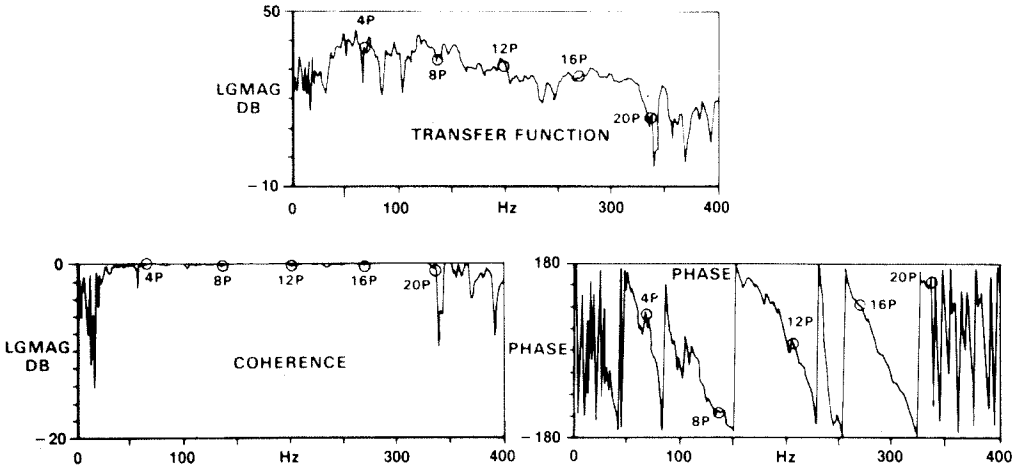

Fig. 15 Repeat tap signature test at point 204 (wing root) with 3-lb mallet raw data.

Table 2 Matrix equation for direct force determination

$$\begin{bmatrix} S_{1R} \\ S_{1I} \\ S_{2R} \\ S_{2I} \\ \cdot \\ \cdot \\ \cdot \\ S_{kI} \end{bmatrix}_n = \begin{bmatrix} T_{11}\cos\phi_{11}, & -T_{11}\sin\phi_{11}, & T_{12}\cos\phi_{12}, & -T_{12}\sin\phi_{12} & \cdots & -T_{1k}\sin\phi_{1k} \\ T_{11}\sin\phi_{11}, & T_{11}\cos\phi_{11}, & T_{12}\sin\phi_{12}, & T_{12}\cos\phi_{12} & \cdots & T_{1k}\cos\phi_{1k} \\ T_{21}\cos\phi_{21}, & -T_{21}\sin\phi_{21}, & T_{22}\cos\phi_{22}, & -T_{22}\sin\phi_{22} & \cdots & -T_{2k}\sin\phi_{2k} \\ T_{21}\sin\phi_{21}, & T_{21}\cos\phi_{21}, & \cdots & & & T_{2k}\cos\phi_{2k} \\ \cdot & \cdot & \cdot & & & \cdot \\ \cdot & \cdot & \cdot & & & \cdot \\ \cdot & \cdot & \cdot & & & \cdot \\ T_{kI}\sin\phi_{kI}, & T_{kI}\cos\phi_{kI}, & \cdots & & & T_{kk}\cos\phi_{kk} \end{bmatrix} \times \begin{bmatrix} F_{1R} \\ F_{1I} \\ F_{2R} \\ F_{2I} \\ \cdot \\ \cdot \\ \cdot \\ F_{KI} \end{bmatrix}_n$$

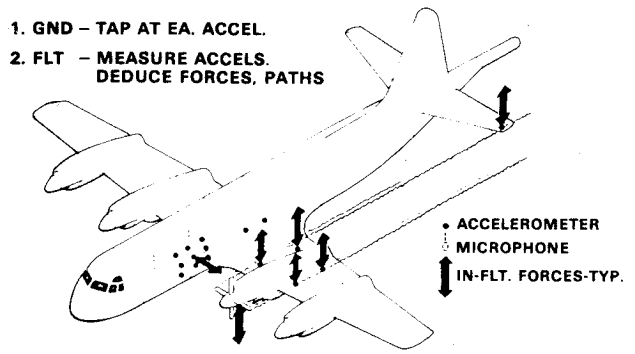

Fig. 16 Direct force measurement.

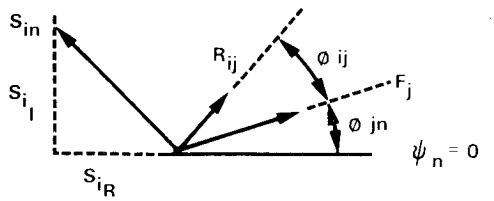

Fig. 17 Propeller signatures determined and expressed in complex form as reals and imaginaries.

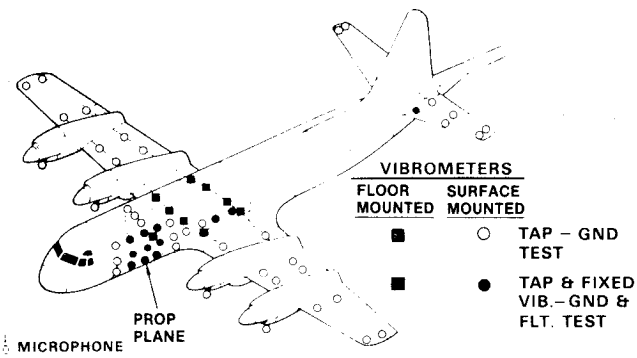

Fig. 18 Indirect determination of slip-stream forces on wing; also direct, shell.

the sum of the cross transfer terms. The next and more logical is to select a grid of sensors that represents the most important terms (largest forces) and to account for the cross transfer as well as self terms in this grid. This selection gives a matrix representation

$$[R] = [T]\,[F] \tag{3}$$

where the number of forces§ determined at each harmonic can be no greater than the number of sensors. These become a *representative* set of forces, a set that represents *all* the excitations in that it produces the observed responses.

The in-flight sensor responses $[R]$ include the effects of all propellers. At each sensor i the response is the vector sum of the propeller signatures,

$$R_i = \sum_{1}^{n} S_{in} \tag{4}$$

where S_{in} is the signature at i of the nth propeller.[8]

To obtain the effect of an individual propeller, n, $[R]$ is replaced by $[S]_n$ of that propeller. This can be considered equivalent to feathering the other propellers.

§Or force distributions, if the methods of the generalized inverse are used.[17]

The propeller signatures are determined and expressed in complex form as reals and imaginaries, subscripts R and I, (Fig. 17).

Then

$$S_{iR} = \Sigma F_j T_{ij} \cos(\phi_{ij} + \phi_{jn}) \qquad \text{including } i=j \tag{5}$$

$$S_{iI} = \Sigma F_j T_{ij} \sin(\phi_{ij} + \phi_{jn}) \qquad \text{including } i=j \tag{6}$$

Expanding Eqs. (5) and (6) and expressing $F_j \cos\phi_{jn} = F_{jR}$, $F_j \sin\phi_{jn} = F_{jI}$, the matrix form is shown in Table 2.

This is

$$[S] = [T]\,[F]$$

Premultiplying by $[T]^T$ and inverting,

$$[F] = [T^T T]^{-1}\,[T^T]\,[S] \tag{7}$$

This is the equation for determining the excitation forces from each propeller separately.

The sensor arrangement shown in Fig. 16 can be used to study the sources/paths of Table 1 by using structural and propeller signatures in Eq. (7)

1) to determine the vibratory wing bending and torsion moments about and along the No. 2 nacelle associated with the slip-stream forces of the No. 2 propeller from the four wing-mounted vibrometers (note that the vibratory inputs from the other propellers have been removed by use of the propeller signatures);

2) to determine the vibratory vertical forces on the propeller from the vibrometer on the propeller gearbox;

3) to determine four different 9-point grids of forces and phases on the left side of the fuselage near the propeller plane; this one 9-point grid for each propeller telling a great deal about the waveforms and phase as well as the spatial distribution of the waveforms from the propellers;

4) to show two representative forces associated with the two vibrometers on the fuselage shell over the wing, including the amount contributed by each propeller;

5) to show representative forces on the stabilizer due to each of the four propellers; the slip-stream effects from the inboard propellers can be inferred from the difference;

6) to accomplish the above for as many multiples of the blade passage frequency as are consistent with the test data accuracy.

The same objectives can also be accomplished, and extended to slip-stream forces about all four nacelles, with indirect sensing. Indirect sensing, as discussed in the following, also permits use of in-cabin instrumentation, with considerable saving in cost.

Indirect Force Analysis

The indirect technique is illustrated in Fig. 18. The intention here is to measure the slip-stream forces on the wing behind all four propellers. Four vibrometers are installed on the cabin floor over the wing, one for each force position associated with one propeller. Their locations are selected during ground tests to show maximum response to slip-stream-related wing excitations behind all four propellers, and minimum response to fuselage shell and tail excitations. The response patterns should be different for each force if the transfer matrix is to be invertible. Vibrometers should also be installed on the shell and in the tail. They will show whether forces at either of these locations have produced significant response in the floor sensors. In any case, they are needed to determine the other excitations producing noise in the cabin.

In the ground signature tests, forces are applied, as before, at positions selected to represent the propeller or slip-stream force applications. The sensors are located in the cabin. The

Table 3 Matrix equation for indirect force determination

$$\begin{bmatrix} S_{1R} \\ S_{1I} \\ S_{2R} \\ S_{2I} \\ S_{3R} \\ S_{3I} \\ S_{4R} \\ S_{4I} \end{bmatrix} = \begin{bmatrix} T_{1a}\cos\phi_{1a}, & -T_{1a}\sin\phi_{1a}, & T_{1b}\cos\phi_{1b}, & -T_{1b}\sin\phi_{1b}, & T_{1c}\cos\phi_{1c}, & -T_{1c}\sin\phi_{1c}, & T_{1d}\cos\phi_{1d}, & -T_{1d}\sin\phi_{1d} \\ T_{1a}\sin\phi_{1a}, & T_{1a}\cos\phi_{1a}, & T_{1b}, & & & & & T_{1d}\cos\phi_{1d} \\ T_{2a}\cos\phi_{2a}, & -T_{2a}\sin\phi_{2a} & - & - & - & - & - & -T_{2d}\sin\phi_{2d} \\ T_{2a}\sin\phi_{2a}, & T_{2a}\cos\phi_{2a} & - & - & - & - & - & T_{2d}\cos\phi_{2d} \\ - & - & - & - & - & - & - & - \\ - & - & - & - & - & - & - & - \\ T_{4a}\cos\phi_{4a}, & -T_{4a}\sin\phi_{4a}, & T_{4b}\cos\phi_{4b} & - & - & - & - & -T_{4d}\sin\phi_{4d} \\ T_{4a}\sin\phi_{4a}, & T_{4a}\cos\phi_{4a}, & T_{4b}\sin\phi_{4b} & - & - & - & - & T_{4d}\cos\phi_{4d} \end{bmatrix} \times \begin{bmatrix} F_{aR} \\ F_{aI} \\ F_{bR} \\ F_{bI} \\ F_{cR} \\ F_{cI} \\ F_{dR} \\ F_{dI} \end{bmatrix}$$

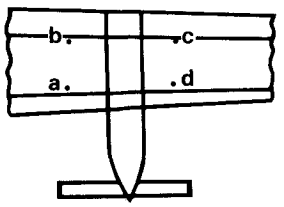

Fig. 19 Selected force points behind propeller no. 1.

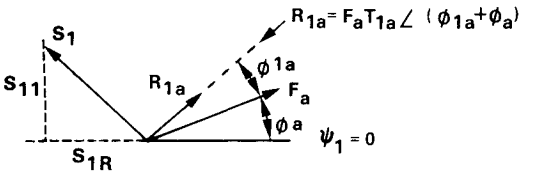

Fig. 20 Forces phased with respect to $\psi_1 = 0$.

mathematical relations are as in Eqs. (1-6) and Table 2, except that in the indirect determinations $i \neq j$.

Let i, the sensors, be numbered 1-4. Let the force points be a-d behind prop No. 1, e be behind prop No. 2, etc. (Fig. 19). Then the signatures at sensors 1-4 are S_1-S_4, and the forces behind the No. 1 prop are F_a-F_d. The forces $F_{a\text{-}d}$ are now phased with respect to $\psi_1 = 0$, the time at which propeller No. 1 passes the reference position. Similarly the forces $F_{e\text{-}h}$ behind prop No. 2 will be phased with respect to $\psi_2 = 0$, etc. (Fig. 20).

$$S_{1R} = F_a T_{1a}\cos(\phi_a + \phi_{1a}) + F_b T_{1b}\cos(\phi_b + \phi_{1b}) + F_c T_{1c}\cos(\phi_c + \phi_{1c}) + F_d T_{1d}\cos(\phi_d + \phi_{1d}) \quad (8)$$

$$S_{1I} = F_a T_{1a}\sin(\phi_a + \phi_{1a}) + F_b T_{1b}\sin(\phi_b + \phi_{1b}) + \text{----------} \quad (9)$$

Expanding Eqs. (8) and (9) and expressing $F_a\cos\phi_a = F_{aR}$, $F_a\sin\phi_a = F_{aI}$, the matrix form is shown in Table 3.

This is $[S] = [T][F]$. Premultiplying, $[T^T][S] = [T^T T][F]$, $[F^T T]^{-1}[T^T][S] = [F]$, therefore

$$\underset{8\times 1}{\begin{Bmatrix} F \\ a\text{-}d \end{Bmatrix}} = \begin{bmatrix} T^T T \\ a\text{-}d\ a\text{-}d \end{bmatrix}^{-1} \times \begin{bmatrix} T^T \\ a\text{-}d \end{bmatrix} \times \underset{8\times 1}{\begin{Bmatrix} S \\ \text{prop 1} \end{Bmatrix}} \quad (10)$$

Similarly

$$\begin{Bmatrix} F \\ e\text{-}h \end{Bmatrix} = \begin{bmatrix} T^T T \\ e\text{-}h \end{bmatrix}^{-1} \times \begin{bmatrix} T^T \\ e\text{-}h \end{bmatrix} \times \begin{Bmatrix} S \\ \text{prop 2} \end{Bmatrix} \quad (11)$$

$$\begin{Bmatrix} F \\ i\text{-}l \end{Bmatrix} = \begin{bmatrix} T^T T \\ i\text{-}l \end{bmatrix}^{-1} \times \begin{bmatrix} T^T \\ i\text{-}l \end{bmatrix} \times \begin{Bmatrix} S \\ \text{prop 3} \end{Bmatrix} \quad (12)$$

$$\begin{Bmatrix} F \\ m\text{-}p \end{Bmatrix} = \begin{bmatrix} T^T T \\ m\text{-}p \end{bmatrix}^{-1} \times \begin{bmatrix} T^T \\ m\text{-}p \end{bmatrix} \times \begin{Bmatrix} S \\ \text{prop 4} \end{Bmatrix} \quad (13)$$

There is one transfer matrix $[T]$ for each propeller. The $[T]$ of Tables 2 and 3 have the same matrices trigonometric relations as the $[\psi]$ matrix used in the propeller signature determination.[8]

If there are more than four floor sensors, then the additional ones may be used for improved accuracy, just as the fifth and sixth sets of propeller phase combinations improve the accuracy of the propeller signature determinations.

Review the ground tests to check for invertibility and conditioning of the $[T]$ matrix, either 8×8 for four sensors or 10×8 for five sensors, etc. The T matrix must always have as many (or more) rows as columns; i.e., at least as many sensors as force points. Use of four force points per prop allows determination of bending and torsion moments plus vertical shear:

$$M_{FB} = (F_d - F_a)\Delta Y, \quad M_{RB} = (F_e - F_b)\Delta Y \quad \text{(bending moments)}$$

$$T_{ib} = (F_d - F_c)\Delta X, \quad T_{ib} = (F_a - F_b)\Delta X \quad \text{(torsion moments)}$$

Total shear is

$$F_a + F_b + F_c + F_d, \quad S_{ob} = F_c + F_d, \quad S_{ib} = F_a + F_b$$

where FB is the front beam, RB is the rear beam, S_{ob} is the outboard shear, and S_{ib} is the inboard shear.

Note that this indirect determination gives a representative force at each point; it tells what set of forces located at these four points (or the corresponding set of moments and shears) would be required to represent *all* the oscillatory forces (except those already subtracted) for that propeller affecting those sensors. For example, the effect of the outboard propeller's slip-stream may be modified significantly by induced aileron motions. This effect will show up in the size of the outboard representative forces as compared with the inboard forces.

It is convenient to make the analyses in terms of the equivalent four forces. It is then desirable to transform the forces to moments before making physical interpretation of the results. Note that the summing and differencing should be made separately on the real and imaginary forces before they are combined into vector moments, torsions, and shears.

Concluding Remarks

The need for large reductions of cabin vibration and noise, as compared with previous propeller airplane experience, requires that every source and every path by which propeller-induced vibration and noise enter the cabin be considered.

A source/path propeller excitation matrix has been presented herein, with rough evaluations. Low-cost, convenient experimental and analytical techniques are described for evaluating the excitations—propeller input forces on the fuselage shell, slip-stream-induced forces and moments on the wing and tail, and oscillatory forces on the propeller—and for evaluating the contributions of each, separately, to the vibration and noise in the cabin. With the excitation forces and responses evaluated in magnitude and phase, design approaches to the goal of making the turbopropeller aircraft vibroacoustic environment competitive with turbofan aircraft can be enunciated logically.

The techniques described make use of structural signatures in ground tests to relate forces with vibrations or noise, and of propeller signatures in flight test to determine the vibroacoustic contributions of individual propellers. Knowing these, the excitation forces due to the individual propeller can be deduced by the relations shown.

An advantage of the measurement techniques is that the flight portion can be accomplished with *in-cabin* instrumentation. This permits exploratory research that was once prohibitively expensive to be performed safely at low cost.

References

[1] Dugan, J.F. et al., "The NASA High-Speed Turboprop Program," SAE Tech. Paper 801120, Oct. 1980.

[2] Goldman, D.E. and Von Gierke, H.E., "The Effects of Shock and Vibration on Man," Naval Medical Research Institute Lecture and Review Series 60-3, Jan. 1960; see also, American Standards Association Rept. ASA 53-W-39.

[3] Revell, J.D., Balena, F.J., and Koval, C.R., "Analytical Model for Study of Interior Noise Control for High-Speed Propeller Driven Aircraft," AIAA Paper 80-1000, June 1980.

[4] Balena, F.J., Revell, J.D., and Koval, C.R., "Analytical Study of Interior Noise Control by Fuselage Design Techniques on High Speed Propeller Driven Aircraft," AIAA Paper 80-1001, June 1980.

[5] Rennison, D.C., Wilby, J.F., and Wilby, E.C., "Prediction of the Interior Noise Levels of High Speed Propeller Driven Aircraft," AIAA Paper 80-0998, June 1980.

[6] Wilby, J.F., Rennison, D.C., and Wilby, E.C., "Interior Noise Control Predictions for High Speed Propeller Driven Aircraft," AIAA Paper 80-0999, June 1980.

[7] Magliozzi, B., "Acoustic Pressures on a Prop-Fan Aircraft Fuselage Surface," AIAA Paper 80-1002, June 1980.

[8] Johnston, J.F., Donham, R.E., and Guinn, W.A., "Propeller Signatures and Their Use," AIAA Paper 80-1035, June 1980.

[9] Farassat, F. and Succi, G.P., "A Review of Noise Prediction Technology with Emphasis on Two Current Methods for Time Domain Calculations," JSV 71:3 Aug. 8, 1980.

[10] Hanson, D.B. and Fink, M.R., "The Importance of Quadrupole Sources in Prediction of Transonic Tip Speed Propeller Noise," JSV, 1979 62 (1), 19-38.

[11] Runyan, H.L., "Noise from a Vibrating Propeller," AIAA Paper 80-1011, June 1980.

[12] Succi, G.P. et al., "Experimental Verification of Propeller Noise Prediction," AIAA Paper 80-0994, June 1980.

[13] Dowell, E.H., "Master Plan for Prediction of Aircraft Interior Noise," AIAA Paper 79-0582, March 1979.

[14] Unruh, J.F., "Structural-Borne Noise Prediction for a Single Engine General Aviation Aircraft," AIAA Paper 80-1037, June 1980.

[15] Ramsey, K.A., "Effective Measurements for Structural Dynamics Testing, Part II," *Sound and Vibration,* April 1976.

[16] Halvorsen, W.G. and Brown, D.L., "Impulse Technique for Structural Frequency Response Testing," *Sound and Vibration,* Nov. 1977, pp. 8-21.

[17] Penrose, R., "A Generalized Inverse for Matrices," *Proceedings of the Cambridge Philosophical Society,* Vol. 51, 1955, pp. 406-413.